The 2nd International Conference on Mechanical System Dynamics (ICMSD2023)
September 1-5, 2023, Beijing, China

The Nonlinear Dynamic Characteristic and Resonant Actuation of Bistable Composite Laminates with MFC

Yuting Liu , Jiaying Zhang * and Qingyun Wang

School of Aeronautic Science and Engineering, Beihang University, Beijing 100190, China
* jiaying.zhang@buaa.edu.cn

Abstract. Bistable structures offer a straightforward means to achieve rapid shape reconfiguration in fields such as morphing aircraft design, flow control, and soft robotics, owing to their unique nonlinear characteristics and strong local stability behavior. Understanding the rapid switching mechanism between stable configurations of bistable laminates is crucial for engineering applications. This study investigates the nonlinear dynamic characteristics of bistable composite laminates with MFC (Macro Fiber Composite) actuators and proposes a resonant actuation method that minimizes energy consumption, enhancing the efficiency and controllability of the configuration switching. An analytical model is developed using the Rayleigh-Ritz method, with static and dynamic models based on the minimum potential energy principle and Hamiltonian principle, respectively. Additionally, considering the mechanical and electrical coupling effects of MFC and utilizing classical laminates theory, accurate geometric solutions for different configurations are obtained by incorporating the actual geometric deformation of the laminates. The nonlinear variation of the natural frequencies of bistable laminates is quantitatively described through backbone curves, revealing frequency hysteresis during frequency sweeps. The critical actuation conditions for bistable laminates actuated by MFC are determined through bifurcation diagrams obtained from forward frequency sweeps. To validate the accuracy of the analytical model under different conditions, comparisons are made with finite element models of bistable laminates created using ABAQUS software.

Keywords: Bistable Laminates, Nonlinear Dynamic, Resonant Actuation.

1 Introduction

Deformable bistable structures hold significant application prospects in engineering fields such as aerospace, energy, and marine industries. In addition, bistable structures possess another prominent feature—they can maintain stability in their equilibrium state without additional power or locking mechanisms. The unique properties of bistable structures, including flexibility, adaptability, and lightweight nature, provide new avenues for the development of intelligent deformable structures. Macro Fiber Composite (MFC) is a type of piezoelectric fiber composite material that exhibits good flexibility and plasticity. They can adhered to different structural surfaces. As an

Supported by "the National Natural Science Foundation of China(12102017,92271104) "and"Research Fund of State Key Laboratory of Mechanics and Control of Mechanical Structures (Nanjing University of Aeronautics and astronautics) (MCMS-E-0522G02)"

actuator, MFC also offers high actuation force, fast response speed, low mass, and thinness. In this study, MFC is used as an actuator for the bistable structures, which facilitates their potential engineering applications in the future.

In 1981, Hyer [1-2] first discovered and theoretically explained the bistability of asymmetric laminates, referring to the transition between two stable configurations as a "snap-through". In 2003, Schultz and Hyer [3-5] conducted modeling and research on bistable composite laminates with MFC by employing the energy variational principle and Rayleigh-Ritz method. They investigated the influence of piezoelectric actuators on the laminate snap-through. Schultz developed a three-step theoretical model for bistable laminates with MFC based on a low-order configuration prediction model. These three steps involved simulating the curing process of the laminates, the MFC attachment process, and the application of voltage to the MFC. Subsequently, they established 4-parameter, 10-parameter, and 16-parameter models, to calculate the deformation and critical voltage for snap-through of [0/90/0/MFC] laminates, respectively. In 2007, Schultz et al. [6] conducted experiments by attaching MFC actuators on both sides of [0/90] bistable laminates for two-way actuation, and the experimental measurements of critical voltage for snap-through were significantly higher than the predicted results of the theoretical model. Gude et al. [7] derived a semi-analytical geometric nonlinear model for bistable composite laminates actuated by piezoelectric ceramic and calculated the critical voltage for piezoelectric actuation. Watts et al. [8] investigated the static and dynamic response of bistable laminates with piezoelectric layers using higher-order shape functions. Senda et al. [9] validated the feasibility of using piezoelectric fibers as actuators through vibration experiments on a cantilever composite beam, showing that the forces generated by piezoelectric fibers can induce a snap-through between the two stable states by resonantly amplifying the structure's amplitude. Casals-Terre et al. [10] proposed the concept of dynamic-actuated bistable structure configuration switching, where rapid switching of bistable structures is achieved by inputting a certain frequency of actuating force. In 2010, Atsuhiko et al. [11] introduced the concept of MFC vibration actuation, which involves applying an alternating voltage to MFC to induce vibration in the laminates. Once the amplitude of the laminates reaches a certain value, the snap-through occurs. Experimental validation showed that orthogonal laminates achieve unidirectional snap-through, while [0/45] laminates achieve bidirectional snap-through. Arrieta [12-14] proposed an actuating strategy using modal frequency excitation to induce large deformation of bistable structures. They designed segmented laminates with MFC excitation to generate vibrations and achieve bidirectional snap-through. The advantage of the vibration-actuated approach is that it enables bidirectional snap-through with lower applied voltages, typically around 300V. Bilgen et al. [15] applied the dynamic actuating strategy to low aspect ratio wings with bistable characteristics, enhancing the aerodynamic performance through dynamic actuation of the bistable structure. Mehrabian et al. [16] employed the maximum value of the frequency response function as the objective function for an optimization algorithm to determine the optimal placement of MFC actuators on flexible fins. They utilized a neural network to accurately fit the discrete data generated by finite element analysis, aiming to maximize the weighted sum of frequency response peaks and achieve the optimal

damping position for the MFC actuators. Victor et al. [17] proposed a multi-objective optimization design method for composite laminates with piezoelectric layers. They utilized a direct search algorithm for optimization, with objectives including maximizing buckling load, inherent frequency under specific vibration modes, minimizing weight, or minimizing applied voltage. Hao et al. [18] investigated the Intrawell and interwell oscillations of asymmetric four-layer cross-ply rectangular laminates actuated by d_{33} MFC actuators. The boundary conditions were set as fixed at the center and free on the four sides. Computational results indicated modifying the amplitude and frequency of the applied voltage can provide better control over the snap-through behavior within a certain range,.

This paper establishes a nonlinear coupled analytical model for MFC and asymmetric composite laminates with arbitrary orientations of piezoelectric fibers. The model is used to simulate the dynamic response of laminates subjected to applied voltage. By investigating the dynamic characteristics of bistable composite laminates, a resonant actuating method with minimal energy input is proposed to achieve more efficient and controllable snap-through behavior. The analytical model is developed using the Rayleigh-Ritz method, and static and dynamic models are established based on the minimum potential energy principle and Hamilton's principle, respectively. Additionally, considering the electromechanical coupling effect of MFC and starting from the actual geometric deformation of the plate structure, the geometric exact solutions for different configurations are derived based on the classical laminate theory incorporating the von Kármán nonlinearity. Nonlinear frequencies of stable configurations are represented using backbone curves to analyze the nonlinear characteristics of the structure and determine the critical actuating conditions for bidirectional snap-through of MFC-actuation bistable laminates. To validate the accuracy of the dynamic model, a comparison is made with the finite element software ABAQUS for bistable laminates. This study employs MFC with cross-ply arrangement is employed to resonantly actuate bistable laminates, and the critical actuating voltage is obtained through bifurcation diagrams varying with frequency.

2 The Model of Bistable Laminates with MFC

2.1 Finite Element Model

This paper utilizes symmetric rectangular composite bistable laminates with two stable configurations having orthogonal principal curvatures. To enhance the energy efficiency of MFC and facilitate the switching between the two stable configurations, an orthogonal arrangement of MFC is employed, as shown in Figure 1. This study employs d_{33} MFC, where the piezoelectric material's polarization aligns with the direction of the piezoelectric fibers, enabling elongation or contraction in the direction perpendicular to the fibers upon the application of an electric field. The laminates have dimensions of length Lx=200mm and width Ly=80mm with a single-layer thickness H of 0.15 mm. The MFC dimensions are given as length PLx=56mm and width PLy=28mm, with a single-layer thickness h_{MFC} of 0.3 mm. The stacking sequence of the laminates is $[0^{MFC}/0/90/90^{MFC}]$.

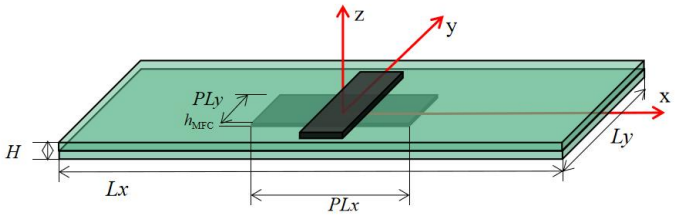

Fig. 1. Schematic diagram of a bistable composite laminate with MFC actuators.

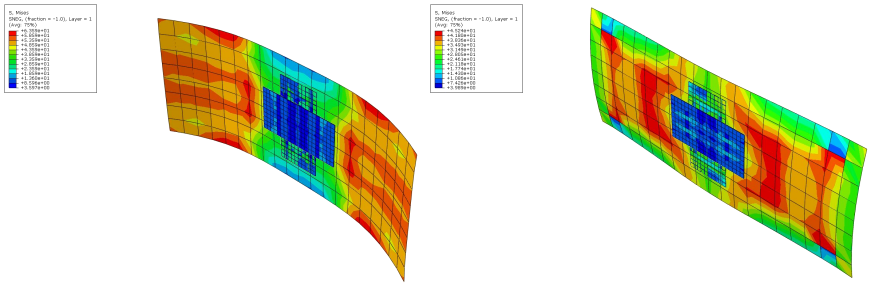

(a) Stable state A (b) Stable state B

Fig. 2. The stable configuration predicted by finite element modal.

To effectively simulate the piezoelectric effect of MFC, the finite element software ABAQUS employs a thermal analogy method. Simulation models of both the MFC and the composite laminate are established using solid and shell elements, respectively. After achieving free convergence of the finite element model, as the model solidifies and cools down, the computed results converge to a cylindrical configuration with bending along the length direction of the laminate, which is referred to as stable configuration A in this study (see Figure 2(a)). If the displacements of the vertices are constrained during the solidification process and then released in subsequent analysis steps, the computed results converge to a cylindrical configuration with bending along the width direction of the laminate, which is denoted as stable configuration B (see Figure 2(b)). By performing a "Static, General" analysis step, the two stable configurations of the bistable laminate are obtained. In this study, the transition from stable configuration A to stable configuration B is referred to as forward loading, while the reverse transition is referred to as backward loading.

2.2 Analytical Model

In the analytical model assumes that the bistable composite laminate is initially in a flat state during manufacturing and cools down to room temperature during solidification. The boundary conditions of the laminate are set as fixed at the center and free on all four sides. The dynamic model of the orthogonal bistable composite

laminate is established using the Hamilton's principle, where the Lagrange equation integrates to zero with respect to time, as shown in Eq. 1.

$$\int_{t_1}^{t_2} \delta(T(t)+W_F(t)-\prod(t))dt=0 \tag{1}$$

where $T(t)$ is kinetic energy, $W_F(t)$ is work done by external forces, and $\prod(t)$ is the total potential energy.

A typical orthogonal bistable laminate consists of two stable cylindrical configurations and one unstable saddle configuration. A Cartesian coordinate system is established with the origin at the center of the laminate, where the x-axis and y-axis are parallel to the length and width of the rectangle laminate, respectively. Due to the thickness of laminate being much smaller than its length and width, the Kirchhoff hypothesis is applicable in this case. The internal strains of the laminate are described as follows

$$\begin{bmatrix} \varepsilon_x \\ \varepsilon_y \\ \gamma_{xy} \end{bmatrix} = \begin{bmatrix} \varepsilon_x^0 \\ \varepsilon_y^0 \\ \gamma_{xy}^0 \end{bmatrix} + z \begin{bmatrix} k_x \\ k_y \\ k_{xy} \end{bmatrix} \tag{2}$$

where

$$\begin{bmatrix} k_x \\ k_y \\ k_{xy} \end{bmatrix} = \begin{bmatrix} -\dfrac{\partial^2 w}{\partial x^2} \\ -\dfrac{\partial^2 w}{\partial y^2} \\ -2\dfrac{\partial^2 w}{\partial x \partial y} \end{bmatrix} \tag{3}$$

Where ε_x , ε_y and ε_{xy} are the mid-plane strains, k_x , k_x and k_x are the bending curvature and twisting curvature of the laminate.

Hyer [2] states that in order to account for large deformations of bistable laminates, the nonlinear Von-Karman terms must be incorporated into the geometric equations. According to the Von-Karman hypothesis, the relationship between the mid-plane strain and displacement of the bistable laminate can be expressed as

$$\varepsilon^0 = \begin{bmatrix} \varepsilon_x^0 \\ \varepsilon_y^0 \\ \gamma_{xy}^0 \end{bmatrix} = \begin{bmatrix} \dfrac{\partial u^0}{\partial x} + \dfrac{1}{2}\left(\dfrac{\partial w}{\partial x}\right)^2 \\ \dfrac{\partial v^0}{\partial y} + \dfrac{1}{2}\left(\dfrac{\partial w}{\partial y}\right)^2 \\ \dfrac{\partial u^0}{\partial y} + \dfrac{\partial v^0}{\partial x} + \dfrac{\partial w}{\partial x}\dfrac{\partial w}{\partial y} \end{bmatrix} \tag{4}$$

u^0, v^0 and w denote the in-plane and out-of-plane displacements, respectively.

During the cooling process of the laminate, residual thermal stresse is generated without any additional external energy input. The positive piezoelectric effect of the MFC converts electrical energy into mechanical energy, resulting in fiber strain. Therefore, the elastic potential energy of the laminate, MFC, and the system can be described by the following equation

$$\Pi_P = \int_{-L_x/2}^{L_x/2}\int_{-L_y/2}^{L_y/2}\left(\frac{1}{2}\begin{bmatrix}\varepsilon^{0\mathrm{T}} & \mathrm{k}^{\mathrm{T}}\end{bmatrix}\begin{bmatrix}\mathrm{A} & \mathrm{B}\\ \mathrm{B} & \mathrm{D}\end{bmatrix}\begin{Bmatrix}\varepsilon^0\\ \mathrm{k}\end{Bmatrix} - \begin{bmatrix}\mathrm{N}_S^{\mathrm{T}} & \mathrm{M}_S^{\mathrm{T}}\end{bmatrix}\begin{Bmatrix}\varepsilon^0\\ \mathrm{k}\end{Bmatrix}\right)\mathrm{dydx} \tag{5}$$

$$\Pi_{MFC} = \int_{-PL_x/2}^{PL_x/2}\int_{-PL_y/2}^{PL_y/2}\left(\frac{1}{2}\begin{bmatrix}\varepsilon^{0\mathrm{T}} & \mathrm{k}^{\mathrm{T}}\end{bmatrix}\begin{bmatrix}\mathrm{A}^{\mathrm{Q}} & \mathrm{B}^{\mathrm{Q}}\\ \mathrm{B}^{\mathrm{Q}} & \mathrm{D}^{\mathrm{Q}}\end{bmatrix}\begin{Bmatrix}\varepsilon^0\\ \mathrm{k}\end{Bmatrix} - \left(\begin{bmatrix}e_{31}\\ e_{32}\\ e_{33}\end{bmatrix}E_3\right)^T\begin{bmatrix}\varepsilon_x^0\\ \varepsilon_y^0\\ \varepsilon_{xy}^0\end{bmatrix}\right)\mathrm{dydx} \tag{6}$$

$$\Pi_{ALL} = \Pi_P + \Pi_{MFC} \tag{7}$$

where L_x and L_x represent the length and width of the laminate, respectively. The length and width of the MFC are represented by PLx and PLy, and it is assumed that they remain constant during the deformation process. A represents the tensile stiffness matrix, B represents the coupling stiffness matrix between tension and bending, and D represents the bending stiffness matrix. N_S and M_S are the force and moment obtained by integrating the residual thermal stresses in the thickness direction of the bistable laminate, which depend on the thermal expansion coefficients of the laminate. e represents the converted piezoelectric coefficient of the MFC, and E_3 represents the electric field intensity in the z-direction of the piezoelectric material. The magnitude of the elastic potential energy of the bistable laminate depends on the assumed displacement functions u^0, v^0 and w the magnitudes of the center surface strains ε^0 and curvatures k represented by these functions.

If the bending curvature of the laminate is a constant, the theoretical model cannot accurately predict the shape of the laminate. Therefore, in this study, it is assumed that the bending curvature of the laminate is not constant. Considering the boundary conditions of the laminate and the characteristics of its deformation symmetric and

antisymmetric, a fourth-order out-of-plane displacement function for the laminate is assumed as

$$w = a(t)x^2 + b(t)y^2 + a_1(t)x^4 + b_1(t)y^4 + e(t)x^2y^2 \tag{8}$$

Assuming that the mid-plane strain of a laminate is related to the cross-sectional shape of the laminate and independent of the out-of-plane displacement function, the mid-plane strain can then be represented by two fourth-order polynomial

$$\begin{aligned} \varepsilon_x^0(t) &= c(t) + c_1(t)y^2 + c_2(t)y^4 + c_3(t)x^2y^2 \\ \varepsilon_y^0(t) &= d(t) + d_1(t)x^2 + d_2(t)x^4 + d_3(t)x^2y^2 \end{aligned} \tag{9}$$

The unknown coefficients $a_i(t)$, $b_i(t)$, $e(t)$, $c_i(t)$ and $d_i(t)$ mentioned are the generalized coordinates in the model. These coefficients can be substituted into the geometric equation (4) to determine the in-plane displacement of the structure. The theoretical model for the given orthogonal asymmetric laminate consists of a total of 13 unknown parameters.

$$u^0(t) = \int \left(\varepsilon_x^0(t) - \frac{1}{2}\left(\frac{\partial w(t)}{\partial x} \right)^2 \right) dx \tag{10}$$

$$v^0(t) = \int \left(\varepsilon_y^0(t) - \frac{1}{2}\left(\frac{\partial w(t)}{\partial y} \right)^2 \right) dy \tag{11}$$

As a result, the kinetic energy of the laminate, MFC, and the system can be expressed as follows, respectively, where ρ_P and ρ_{MFC} represent the densities of the composite material and MFC, respectively.

$$T_P = \frac{1}{2}\rho_P \int_{V_P} \left(\dot{u}^{0^2} + \dot{v}^{0^2} + \dot{w}^2 \right) dV \tag{12}$$

$$T_{MFC} = \frac{1}{2}\rho_{MFC} \int_{V_{MFC}} \left(\dot{u}^{0^2} + \dot{v}^{0^2} + \dot{w}^2 \right) dV \tag{13}$$

$$T_{\mathrm{ALL}} = T_P + T_{MFC} \tag{14}$$

Based on the principle of Hamilton, the Lagrange equation (1), and the displacement function, the equations of motion for the system are derived

$$\mathbf{M_1}\ddot{\mathbf{X}}_\mathbf{1} + \mathbf{D_1}\left(\dot{\mathbf{X}}_\mathbf{1}\right) + \mathbf{K_1}\left(\mathbf{X_1}\right) = \mathbf{F_1} \tag{15}$$

$\mathbf{M}_1$ represents the mass matrix, $\mathbf{D}(\dot{\mathbf{X}}_\mathbf{I})$ represents the damping force, and $\mathbf{K}_\mathbf{I}(\mathbf{X}_\mathbf{I})$ represents the nonlinear elastic force. $\mathbf{F}_\mathbf{I}$ is the external excitation force, which depends on the inertia of the laminate and the intensity of the external excitation.

By utilizing the numerical solver for partial differential equations in MATHEMATICA, the numerical solutions of the partial differential equation system are obtained. It can be seen that two sets of stable solutions representing two stable configurations and one set of unstable solutions representing the unstable configuration resembling a saddle shape, as shown in Figure 3. After obtaining the stable configurations of the bistable laminate, the fundamental frequencies in the deflection direction of the laminate are obtained by performing the Fast Fourier Transform on the decaying displacement of free attenuation vibrations. A comparison between the vertex deflections and fundamental frequencies predicted by the analytical model and the finite element model for the two stable configurations is presented in Table 1, showing satisfactory agreement between the results and validating the accuracy of the analytical model.

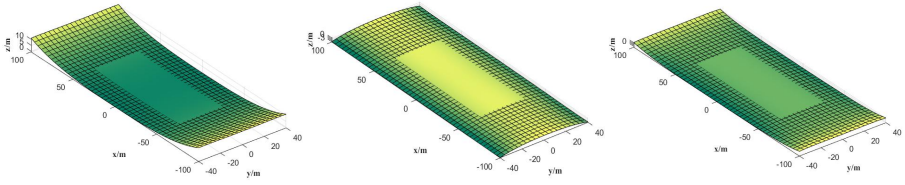

(a) Stable state A (b) Stable state B (c) Unstable state

Fig. 3. The stable configuration predicted by analytical modal.

Table 1. Related results of stable configuration.

	Stable state A		Stable state B	
	Vertex deflection	Fundamental frequency	Vertex deflection	Fundamental frequency
Analytical model	19.134 mm	37.0 Hz	-4.1 mm	83.6 Hz
Finite element model	20.126 mm	36.9 Hz	-3.76 mm	95.833 Hz

2.3 Nonlinear behavior of bistable laminates

The bistable laminated panel, as a representative nonlinear structure, exhibits variations in its natural frequencies in response to external excitation. To facilitate subsequent resonance-actuated investigations, this paper introduces the concept of the backbone curve to characterize and quantify this nonlinear behavior. The frequency response curves of the structure is obtained under different intensities of single-sided harmonic excitation and further connect the resonant peaks of the frequency response curve, from which we extract the backbone curve as depicted in Figure 4. Specifically, The frequency response curves are obtained at excitation amplitudes of

100 V, 300 V, 500 V, 700 V, and 900 V. For relatively lower intensities of external excitation, such as an amplitude of 100 V, the resonant peak in the frequency response curve of the structure shift towards higher frequencies, indicating characteristics of a harden stiffness. As the intensity of the external excitation increases, the natural frequencies of the structure decrease with the increasing excitation intensity. Simultaneously, the resonant peaks in the frequency response curves shift towards lower frequencies, illustrating characteristics of a soften stiffness. The natural frequencies lies between 36 Hz and 37 Hz, reaching a minimum value of 36.2 Hz at an excitation voltage amplitude of 900 V.

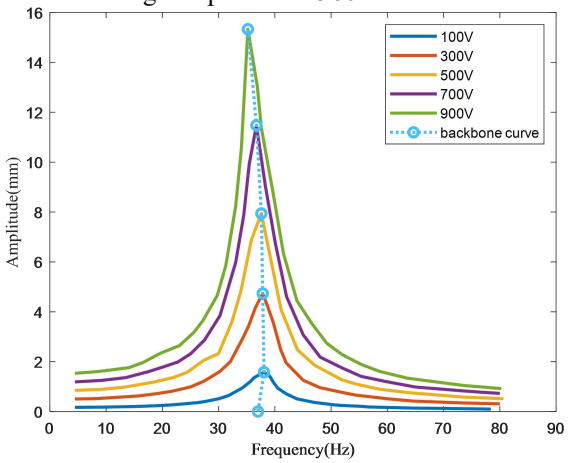

Fig. 4. The backbone curve of analytical model.

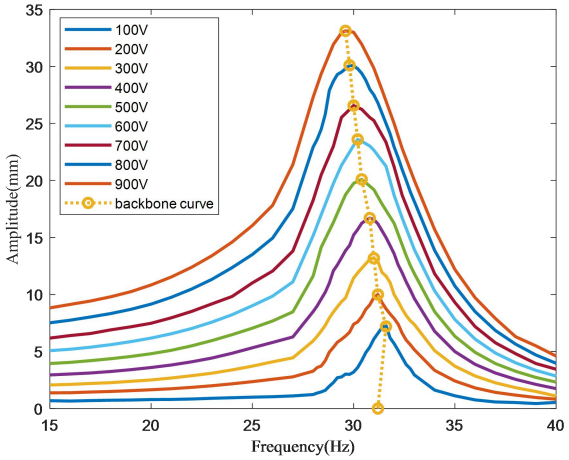

Fig. 5. The backbone curve of test specimen.

The same methodology is applied in the experimental setup to obtain the backbone curve of the test specimen, gradually increasing the excitation amplitude from 100 V

to 900 V, as shown in Figure 5. The observed trend aligns with the predictions of the analytical model, with the natural frequencies between 29.5 Hz and 31.5 Hz. During spring softening, the resonant frequencies of the structure decrease with increasing vibration amplitudes, while during spring hardening, the resonant frequency increase with increasing vibration amplitudes. These characteristics are consistently observed in both theoretical calculations and experimental observations. As the excitation amplitude increases, the structure exhibits a nonlinear behavior transitioning from hardening to softening.

The response of the structure depends not only on the excitation settings but also on the direction of the sweep frequency. As shown in the figure 6, the red curve represents the forward sweep, while the black curve represents the reverse sweep. At an external excitation amplitude of 100 V, the resonant peak bends towards higher frequencies, exhibiting the hardening nonlinear behavior. When the external excitation is 700 V, the resonant peak bends towards lower frequencies, demonstrating softening nonlinear behavior. Moreover, in the forward sweep, starting from low frequencies, the excitation reaches point A_{up}, where the response amplitude abruptly jumps to B_{up}. This phenomenon is known as the sweep up case. Similarly, in the reverse sweep, starting from high frequencies, the excitation reaches point A_{down}, and then jump to B_{down}. The mismatch of resonant peaks in the forward and reverse sweeps is a typical nonlinear dynamic behavior known as frequency hysteresis.

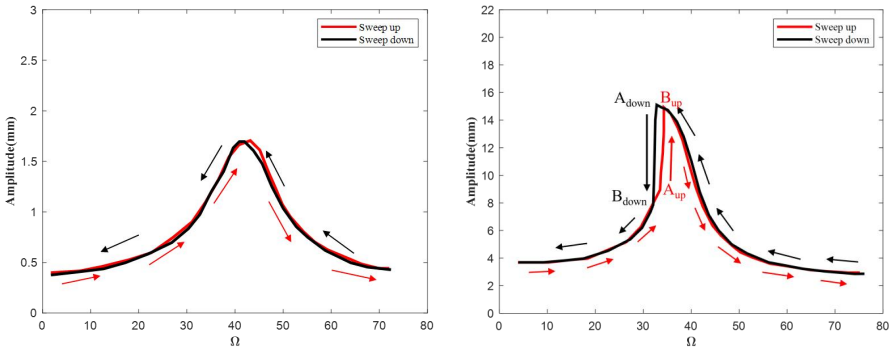

(a) U=100 V (b) U=700 V

Fig. 6. Frequency response curves under different excitation states.

3 Snap-through Actuation

3.1 Quasi-static actuation

Initially, accurate stable configurations with zero voltage and no external load is obtained. The quasi-static loading process is then analyzed using both the analytical model and the finite element model. Figure 7 illustrates the vertex displacement of the laminate in the analytical model with increased applied voltage. The blue curve represents the loading curve starting from the stable state A, with the initial displacement corresponding to the maximum deflection of stable configuration A,

which is a positive value. The loading shape is computed using the Newton-Raphson method by increasing the applied voltage. At a critical voltage point, the vertex displacement undergoes a sudden change, jump to a value opposite in sign to the previous one. This critical voltage point represents the quasi-static critical snap-through voltage, which is 5377 V for forward loading. The red loading curve represents the reverse loading starting from stable state B, and the overall displacement behavior is similar to that of forward loading. The critical snap-through voltage for reverse loading is 855 V.

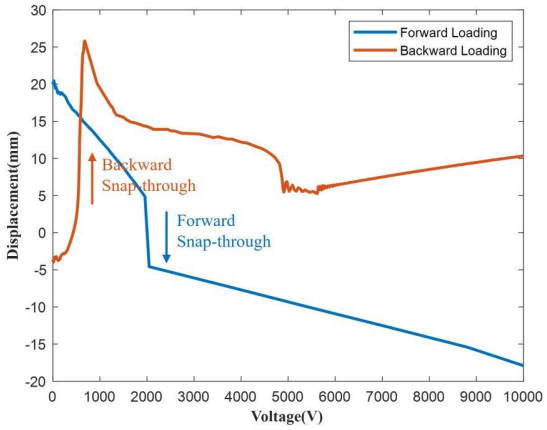

Fig. 7. The static loading displacement curve of analytic model .

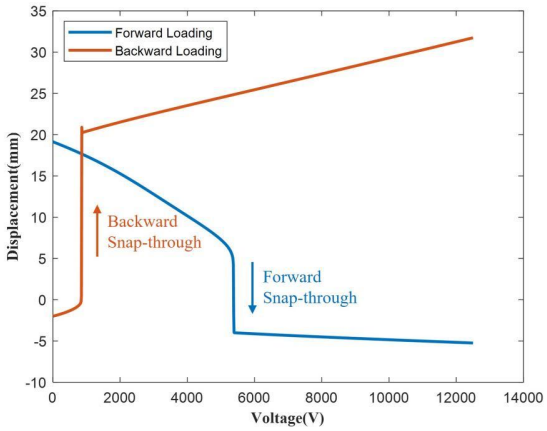

Fig. 8. The static loading displacement curve of finite element model.

Using the same method, the quasi-static snap-through predictions are also performed in the finite element model, as shown in Figure 8. The predicted results of the finite element model show a similar trend to the analytical model in the first half, yielding a critical voltage of 2046 V for the forward loading and 660 V for the reverse loading.

However, in the second half, the trend is significantly different from the results of the analytical model. This is attributed to local buckling occurring in the structure when subjected to higher external loads. The buckling primarily occurs at the location of the MFC attachment, along the direction of MFC's ply orientation. The discrepancy arises mainly from the differences in modeling the elements between the two models and the variations in the connection methods between the MFC and the composite laminate.

3.2 Resonant Actuation

The initial stable configuration of the bistable laminated panel is denoted as stable state A. A harmonic excitation in the form of $U\sin(2\pi\times\Omega\times t)$ is applied from upper MFC, with forward loading. Figure 9 presents two bifurcation diagrams and corresponding displacement curves. Figure 9(a) illustrates the dynamic response as the excitation frequency Ω is set to 36 Hz, while the excitation amplitude varies. Figure 9(b) represents the dynamic response as the excitation amplitude U is fixed at 1100V, while the excitation frequency varies.

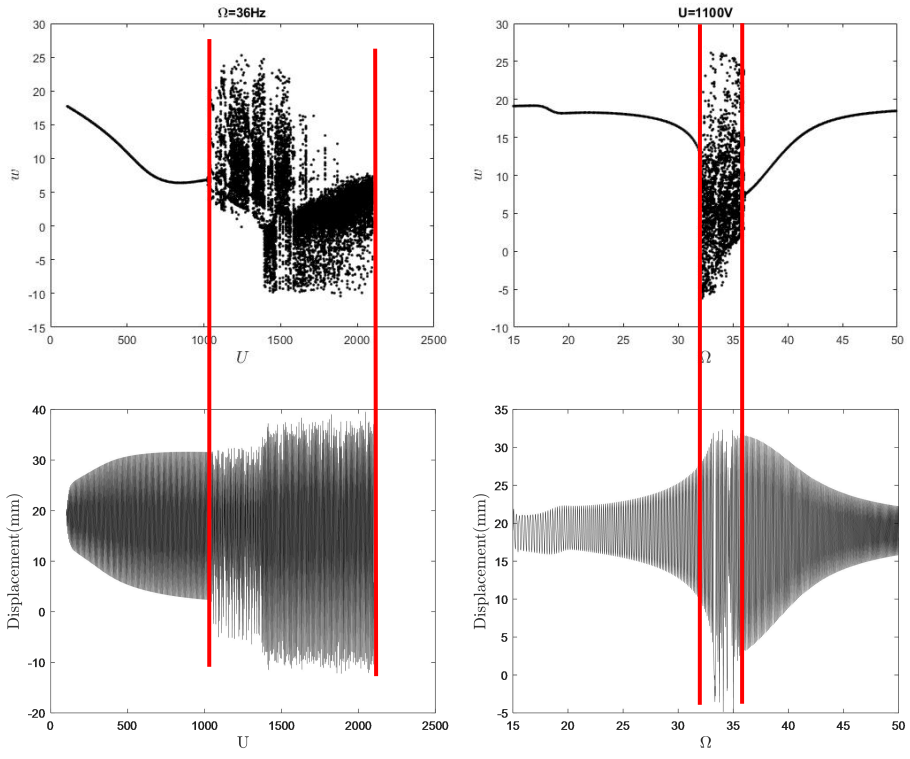

(a) Varies with the excitation amplitude Ω=36 Hz

(b) Varies with the excitation frequency U=700 V

Fig. 9. Bifurcation diagram and displacement curve for excitation amplitude and frequency.

Within the range indicated by the red line, the bifurcation diagrams exhibit chaotic vibrations, corresponding to irregular harmonic motion in the displacement curves. It is noteworthy that variations in both amplitude and frequency lead to significantly different dynamic responses, with the possibility of both periodic and chaotic responses. In Figure 9(a), for smaller excitation amplitudes, the structure demonstrates periodic responses until U reaches 1050 V. Beyond that point, the system exhibits chaotic responses, with occasional regions displaying periodic responses. On the other hand, Figure 9(b) indicates that the structure undergoes chaotic motion in the vicinity of the natural frequency range of 32.4 Hz to 36.1 Hz, while it exhibits periodic motion in regions far from the natural frequency.

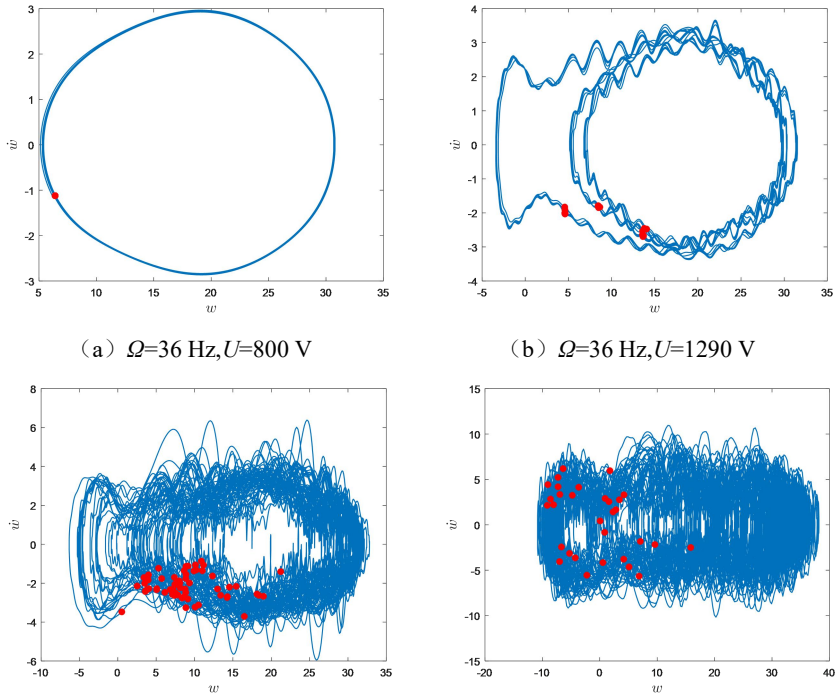

（a）Ω=36 Hz,U=800 V　　（b）Ω=36 Hz,U=1290 V

（c）Ω=36 Hz,U=1400 V　　（d）Ω=36 Hz,U=1700 V

Fig. 10. Phase diagram and Poincaré section.

In order to further investigate the nonlinear dynamic response of the system, it is necessary to analyze the phase space and Poincaré section under certain special conditions. Figure 9 illustrates the dynamic response of a bistable laminate under different loading conditions. Figures 10 (a)-(d) present the phase spaces of the system response at a fixed frequency Ω = 36 Hz, with amplitudes U of 800 V, 1290 V, 1400 V, and 1700 V, respectively, corresponding to the cases shown in Figure 9(a). Figure 10(a) corresponds to the initial periodical vibration, while Figures 10(c) and (d) represent chaotic responses. Figure 10(b) indicates the occurrence of periodic oscillations within a narrow range, known as a periodic window within the chaotic

region. The phase portraits in Figures 10(b)-(c) show structural transitions and oscillations between the two stable configurations. Figures 11(a)-(d) depict the phase spaces at a fixed amplitude U = 1100 V and frequencies of 25 Hz, 33.7 Hz, 36 Hz, and 45 Hz, respectively, corresponding to the scenario in Figure 9(b). In Figures 11(a) and (d), the structure exhibits periodic oscillations, while the phase portraits and Poincaré sections in Figures 11(b) and 11(c) indicate structural transitions occurring within chaos.

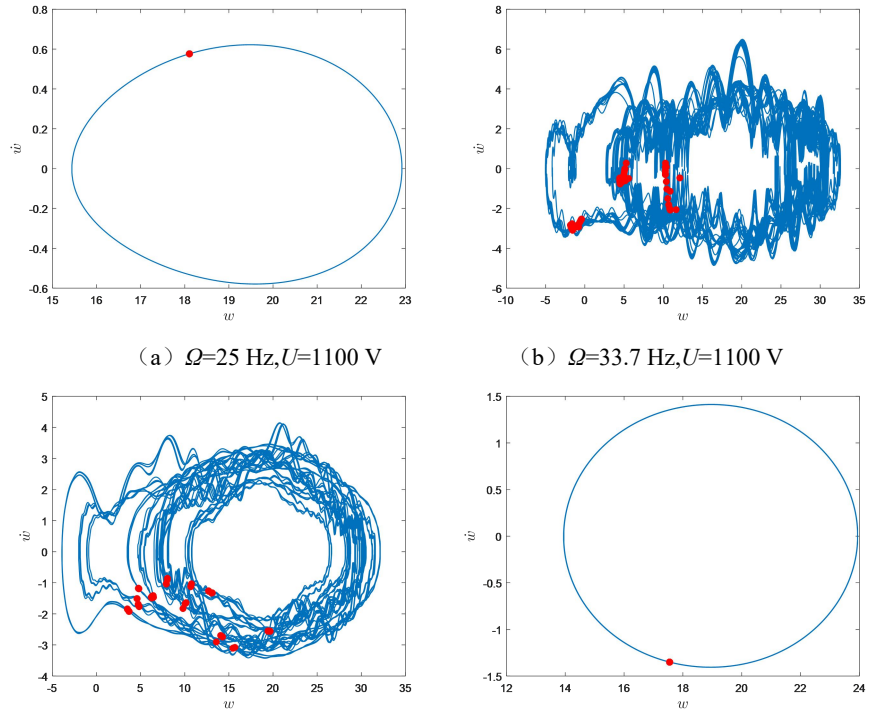

（a）Ω=25 Hz,U=1100 V　　（b）Ω=33.7 Hz,U=1100 V

（c）Ω=36 Hz,U=1100 V　　（d）Ω=45 Hz,U=800 V

Fig. 11. Phase diagram and Poincaré section.

The results demonstrate that the frequency bandwidth of snap-through oscillations in bistable composite laminate plates increases with increasing excitation intensity. Due to the uncertainty of the structural natural frequency under different excitation intensities, in order to determine the critical conditions for forward loading, it is necessary to gradually reduce the amplitude voltage of the excitation and observe the structural response with respect to frequency to determine the critical conditions for forward loading. The critical condition for resonance-actuated snap-through oscillations is obtained when the frequency bandwidth of snap-through oscillations reaches its minimum. Similarly, it can be anticipated that when the excitation amplitude is sufficiently small, the frequency bandwidth of chaotic snap-through oscillations approaches zero, indicating that the structure is unable to complete a

snap-through transition. Figure 12 shows the Poincaré section reveals that the structure consistently undergoes periodic motion around the initial stable configuration at an external excitation amplitude of 880 V. Figure 13 illustrates that the structure exhibits chaotic oscillations at an external excitation amplitude of approximately 890 V and a frequency of 33.5 Hz. Figure 14 shows that the structure undergoes a snap-through transition within the chaotic regime. In this case, the frequency bandwidth of chaotic oscillations is relatively small, suggesting that the critical load for resonance-actuated snap-through transition in the bistable laminate plate is predicted to be 890 V, which is significantly lower than the static actuating voltage of 5377 V.

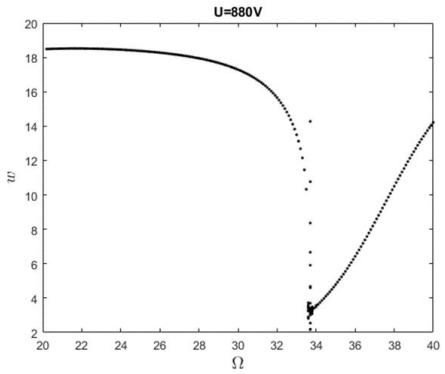

Fig. 12. Bifurcation diagram varies with the excitation frequency.

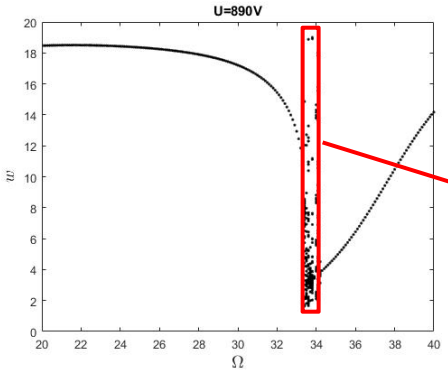

Fig. 13. Bifurcation diagram varies with the excitation frequency.

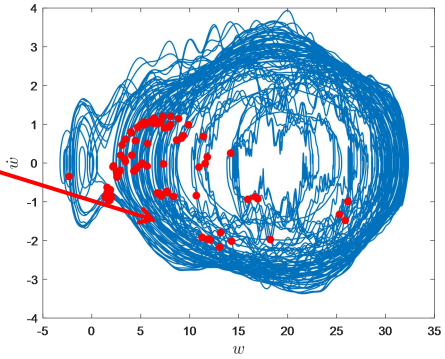

Fig. 14. Phase diagram and Poincaré section.

The initial stable configuration of the bistable laminated panel is denoted as configuration B. By employing the MFC located below the panel, the reverse loading bifurcation diagram is further observed. The excitation amplitude remains constant at 100 V, while the excitation frequency gradually increases from 70 Hz to 90 Hz, as

shown in figure 14. It can be seen from the displacement curve in Figure 15, the structure undergoes periodic vibrations around the stable state B, corresponding to the first half of the bifurcation diagram. When the frequency reaches a range between 74.2 Hz and 82 Hz, the structure undergoes a transition to the stable state A, exhibiting periodic vibrations corresponding to the middle portion of the bifurcation diagram. After reaching 82 Hz, the structure continues to exhibit periodic oscillations around the neighbourhood of the stable state B. The structure exhibits periodic attenuating vibrations both before and after the transition. Using the forward loading method to determine the critical voltage, the smallest region in the bifurcation area corresponds to the critical transition value for reverse loading. In Figure 16, when the external excitation amplitude is 75 V and the resonance region is sufficiently small, this value is considered as the critical actuating voltage. The required voltage of 75 V for resonance actuating is much lower than the static loading of 855 V.

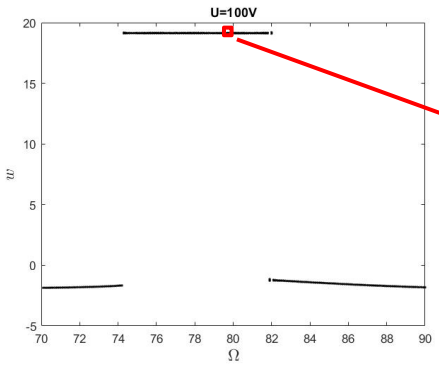

Fig. 14. Bifurcation diagram varies with the excitation frequency.

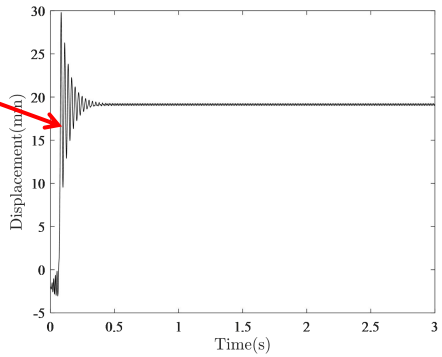

Fig. 15. Displacement curve.

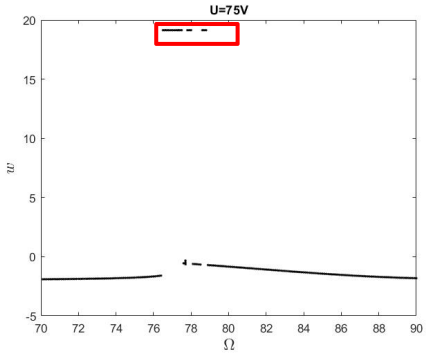

Fig.16. Bifurcation diagram varies with the excitation frequency.

4 Conclusion

This paper proposed a nonlinear coupled analytical model, which predicts a accurate deformation for a MFC actuated bistable laminate plate. Compared to finite element analysis, the analytical model significantly reduces computation time while ensuring accuracy. Departing from the previous assumption that the curvature of the laminate plate is constant, the model considers the actual geometric deformation of the plate. The typical nonlinear behaviors observed during the frequency sweep process of the bistable laminate plate are analyzed. The nonlinearity of the structure is graphically represented by the backbone curve between natural frequencies and excitation. Both theoretical calculations and experimental results exhibit consistent characteristics: the excitation amplitude increases, the structure demonstrates nonlinear behavior transitioning from spring hardening to softening.

In the resonant actuating response, the two MFC patches on the bistable laminate plate are subjected to voltages. Under forward loading, the response is primarily characterized by periodic oscillations and chaos, while under reverse loading, the response mainly exhibits damped periodic motion. By analyzing the bifurcation diagram of the structural response as the excitation frequency changes, the critical voltage for resonant actuating is obtained when the resonance region is minimized. Results show that the required voltage amplitudes for resonant actuating are significantly lower than the voltages required for quasi-static actuating.

References

1. Hyer M W. Some observations on the cured shape of thin unsymmetric laminates[J]. Journal of Composite Materials, 1981, 15(2): 175-194.
2. Hyer MW. Calculations of the Room-Temperature Shapes of Unsymmetric Laminates two. Journal of Composite Materials. 1981;15(4):296-310.
3. Schultz, M.R., and Hyer, M.W.: ‘Snap-through of unsymmetric cross-ply laminates using piezoceramic actuators’, Journal of Intelligent Material Systemsand Structures, 2003, 14, (12), pp. 795.
4. Schultz, M.R., Hyer, M.W., Brett Williams, R., Keats Wilkie, W., and Inman, D.J.: ‘Snap-through of unsymmetric laminates using piezocomposite actuators’, Composites science and technology, 2006, 66, (14), pp. 2442-2448.

5. Schultz, M.R., and Hyer, M.W.: 'A morphing concept based on unsymmetric composite laminates and piezoceramic MFC actuators', AIAA Paper, 2004, 1806, pp. 19-22.
6. Schultz, M.R., Wilkie, W.K., and Bryant, R.G.: 'Investigation of self-resetting active multistable laminates', Journal of Aircraft, 2007, 44, (4), pp. 1069-1076.
7. Gude, Maik & Hufenbach, W. & Kirvel, Christian. Piezoelectrically driven morphing structures based on bistable unsymmetric laminates. Composite Structures - COMPOS STRUCT. 93. 377-382(2011).
8. Taki, Mohammad Sina & Tikani, Reza & zisei-rad, Saeed & Firouzian-Nejad, Ahmad. Dynamic responses of cross-ply bi-stable composite laminates with piezoelectric layers. Archive of Applied Mechanics. 86(2016).
9. Senba, A., Ikeda, T., and Ueda, T.: 'A two-way morphing actuation of bi-stable composites with piezoelectric fibers'. Proc. 51st AIAA/ASME/ASCE/AHS/ASC Structures, Structural Dynamics, and Materials Conference, Orlando, Florida, 2010.
10. Casals-Terre J, Fargas-Marques A, Shkel A M. Snap-action bistable micromechanisms actuated by nonlinear resonance[J]. Journal of microelectro mechanical systems, 2008, 17(5): 1082-1093.
11. Casals-Terre J, Fargas-Marques A, Shkel A M. Snap-action bistable micromechanisms actuated by nonlinear resonance[J]. Journal of microelectro mechanical systems, 2008, 17(5): 1082-1093.
12. Arrieta A F, Bilgen O, Friswell M I, et al. Dynamic control for morphing of bi-stable composites[J]. Journal of Intelligent Material Systems and Structures, 2013, 24(3): 266-273.
13. Arrieta A F, Wagg D J, Neild S A. Dynamic snap-through for morphing of bi-stable composite plates[J]. Journal of Intelligent Material Systems and Structures, 2011, 22(2): 103-112.
14. Arrieta A F, Van Gemmeren V, Anderson A J, et al. Dynamics and control of twisting bi-stable structures[J]. Smart Materials and Structures, 2018, 27(2): 025006.
15. Bilgen O, Arrieta A F, Friswell M I, et al. Dynamic control of a bistable wing under aerodynamic loading[J]. Smart materials and structures, 2013, 22(2): 025020.
16. Mehrabian, Ali & Yousefi-Koma, Aghil. A novel technique for optimal placement of piezoelectric actuators on smart structures. Journal of the Franklin Institute. 348. 12-23(2011).
17. Franco Correia, Victor & Madeira, J. & Araújo, A.L. & Soares, Cristóvão Manuel. Multiobjective design optimization of laminated composite plates with piezoelectric layers. Composite Structures. 169 (2016).
18. Hao, Y.X. & Bai, C.P. & Zhang, Wei & Liu, L.T. & Yang, Shaowu. Intrawell and interwell oscillations for bi-stable cross-ply laminates actuated by MFC under oscillating impulse voltages. International Journal of Non-Linear Mechanics. 143. 104025(2022)..